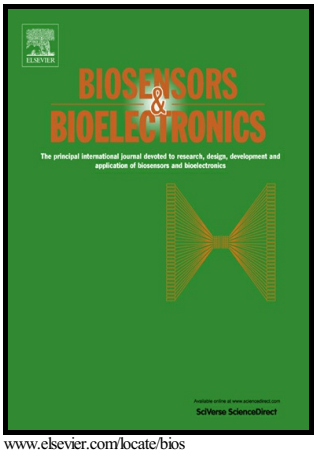

www.elsevier.com/locate/bios

A Dual-color Fluorescent Biosensing Platform Based on WS_2 Nanosheet for Detection of Hg^{2+} and Ag^{+}

Xianwei Zuo, Huige Zhang, Qian Zhu, Weifeng Wang, Jie Feng, Xingguo Chen

PII: S0956-5663(16)30473-0
DOI: http://dx.doi.org/10.1016/j.bios.2016.05.044
Reference: BIOS8734

To appear in: *Biosensors and Bioelectronic*

Received date: 14 March 2016
Revised date: 4 May 2016
Accepted date: 13 May 2016

Cite this article as: Xianwei Zuo, Huige Zhang, Qian Zhu, Weifeng Wang, Jie Feng and Xingguo Chen, A Dual-color Fluorescent Biosensing Platform Based on WS_2 Nanosheet for Detection of Hg^{2+} and Ag^{+}, *Biosensors and Bioelectronic,* http://dx.doi.org/10.1016/j.bios.2016.05.044

A Dual-color Fluorescent Biosensing Platform Based on WS_2 Nanosheet for Detection of Hg^{2+} and Ag^{+}

Xianwei Zuo,[†,‡,▽,£] Huige Zhang,[†,‡] Qian Zhu,[†,‡] Weifeng Wang,[†,‡] Jie Feng,[†,‡] Xingguo Chen,[†,‡,§,*]

[†] State Key Laboratory of Applied Organic Chemistry, Lanzhou University, Lanzhou 730000, China

[‡] Department of Chemistry, Lanzhou University, Lanzhou 730000, China

[§] Key Laboratory of Nonferrous Metal Chemistry and Resources Utilization of Gansu Province, Lanzhou 730000, China

[▽] Key Laboratory of Sensor and Sensor Technology，Gansu Province, Lanzhou 730000, China

[£] Institute of Sensor Technology, Gansu Academy of Sciences, Lanzhou 730000, China

***Corresponding Author**

Xingguo Chen, Professor,

Tel: 86-931-8912763

Fax: 86-931-8912582

E-mail: chenxg@lzu.edu.cn

Abstract: In this work, an effective dual-color fluorescent biosensing platform based on WS_2 nanosheets was developed for homogeneous detection of Hg^{2+} and Ag^{+}. This sensing platform was constituted by exploiting the fluorescence quenching ability of WS_2 nanosheets and the interactions between WS_2 nanosheets and DNA molecules. ~~Without~~

~~adding~~ In the absence of additional any masking agents, the biosensor could achieve detection of Hg^{2+} and Ag^{+} in the same solution by ~~respectively~~ monitoring ~~the~~ fluorescence intensity changes ~~of the sensing system~~ at 525 nm and ~~/~~583 nm, respectively. ~~Taking advantage of this sensing platform,~~ Hg^{2+} and Ag^{+} were selectively detected in the concentration range from 6.0 nM ~~to~~ 650.0 nM and 5.0 nM ~~to~~ 1000.0 nM, respectively, with the detection limit of 3.3 nM and 1.2 nM, respectively. It was also demonstrated that the WS_2 nanosheet-based sensing platform was suitable for the simultaneous detection of Hg^{2+} and Ag^{+} in drinking water，serum and cell lysate samples. Moreover, ~~this research revealed that~~ the possible mechanism of fluorescence quenching by WS_2 nanosheets was revealed to be related to static quenching, dynamic quenching, and Förster resonant energy transfer (FRET). ~~was the coexistence of both dynamic and static quenching~~. This work extended the application of WS_2 nanosheets to environmental monitoring and medical diagnosis.

Key words: WS_2 nanosheet; dual-color fluorescent biosensor; Hg^{2+}; Ag^{+}; homogeneous detection.

1. Introduction

Mercury ions (Hg^{2+}) and silver ions (Ag^{+}) are two of highly toxic metal ions and widespread environmental pollutants ~~in the environment~~,

which can cause serious and permanent damage to the environment and humans ~~body~~ even at low concentrations (Wang, et al., 2009; Tan, et al., 2010; Zhu, et al., 2014). More seriously, through polluted water sources, Ag^{+} and Hg^{2+} can accumulate to agricultural products and aquatic products, ~~and thereby~~ entering the food chain of humans. In case of long time exposure in the environment of existing Ag^{+} and Hg^{2+}, humans may cause slowly progressing physical ~~or~~ and neurological degenerative ~~processes~~ diseases. (Aragay, et al., 2011; Ratte, 1999). Therefore, the detection of Hg^{2+} and Ag^{+} is very important in the fields of environmental monitoring, food safety and clinical diagnosis.

Conventional methods for the determination of Hg^{2+} and Ag^{+} include plasma mass spectrometry (ICP-AES) (Jitaru, et al., 2003), atomic absorption/emission spectroscopy (Pu, et al., 1998; Li, et al., 2011), and polarography (Cizdziel, et al., 2004)~~, and so on~~. These methods often require complex operation, time-consuming analysis and sophisticated equipment, ~~which made them limit wide applications in~~ making them unavailable in many resource-limited settings (Zhu, et al., 2014). To overcome these drawbacks, the fluorescent sensors ~~got greatly~~ have been developed due to their high sensitivity, fast analysis, and simplicity. Since T-T mismatches selectively captured Hg^{2+} to form T-Hg(II)-T base pairs and C-C mismatches exclusively recognized Ag^{+} to form C-Ag(I)-C base pairs were reported (Miyake, et al., 2006; Ono, et al., 2008)， much effort

have been devoted toward the design of DNA-based fluorescent sensors for the detection of Hg^{2+} or Ag^{+} in water, drugs, food and clinical samples(Zhan, et al., 2015; Zhang, et al., 2015; Bian, et al., 2014; Zhang, et al., 2010; Wen, et al., 2010; Liu, et al., 2012; Wu, et al., 2016). Although these assays are respectable innovation and high sensitivity, most of them focus on single metal ion detection. However, Hg^{2+} and Ag^{+} are usually coexisting in water, soil and even biological systems (Chu, et al., 2002). For the coexisting systems of Hg^{2+} and Ag^{+}, these assays need different detection methods and experimental conditions to simultaneous detection of Hg^{2+} and Ag^{+}, which increase the complexity and inconvenience of these assays. To satisfy the practical requirements of analysis of real samples, several attempts have been ~~carried out~~ made to achieve the ~~for~~ simultaneous detection of Hg^{2+} and Ag^{+} (Wang, et al., 2014; Lin, et al., 2011; Lin, et al., 2010; Zhang, et al., 2015; Xia, et al., 2014; Wang, et al., 2013; Shi, et al., 2010). ~~But above~~ However, these assays suffer certain limitations in practical applications, such as using masking agents, low sensitivity, and complexity. Therefore, it is still a great challenge to achieve simple, sensitive, and simultaneous detection of Hg^{2+} and Ag^{+} in real samples.

In recent years, transition metal dichalcogenides (TMDCs) ~~as~~ ,which are two-dimensional (2D) layered nanomaterials that are analogous to graphene, were getting more and more attention due to their high specific

surface area, remarkable electronic property, unique optical and excellent catalytic property (Coleman, et al., 2011; Chhowalla, et al.,2013; Zhu, et al., 2013). Layered tungsten disulfide (WS_2) nanosheets are ~~is~~ one of the newly emerging TMDCs, which consist~~s~~ of S-W-S sandwiche~~s~~ structures. WS_2 nanosheets have been ~~has~~ received intensive research in the field of catalyst, field-effect transistor, lithium ion battery, and so on (Zeng, et al., 2011). WS_2 nanosheets have ~~has~~ been reported to allow self-assembly of thiolated compounds on its surface (Chou, et al., 2013). This indicates one major advantage of WS_2 nanosheets over graphene in facile surface modification, which make WS_2 nanosheets hold great potential in biosensing applications. However, up to now, only few efforts have been devoted to explore the applications of WS_2 nanosheets in bio-sensing ~~biomolecular detection~~ (Xi, et al., 2014; Yuan, et al., 2014; Zhao, et al., 2010; Qin, et al., 2015; Huang, et al., 2014; Lin, et al., 2014). Therefore, there is an urgent need to explore ~~the~~ new applications of WS_2 nanosheet in the area of biosensor. It has been reported that WS_2 nanosheets can adsorb and quench dye-labeled single-stranded DNA (ssDNA) probes. When the adsorbed ssDNA probes hybridize with complementary strands to form double-stranded DNA (dsDNA) with its target, the fluorescence is recovered, because the probes are released from WS_2 nanosheets (Yuan, et al., 2014; Moses, et al., 2009).~~when the probe formed a duplex with its target, which released the probe from WS_2 nanosheet (Yuan, et al., 2014;~~

~~Moses, et al., 2009).~~ More importantly, WS_2 nanosheets exhibit robust quenching efficiency. ~~a notable merit that the quenching efficiency is very robust.~~ (Xi, et al., 2014). Inspired by these previous findings, we believe that WS_2 nanosheets can be coupled with dye-labeled oligonucleotide probes to develop a quenching-and-recovery- based fluorescent biosensor for Hg^{2+} and Ag^{+} detection. Although graphene oxide(GO)-based fluorescent biosensors have been reported for the detection of Hg^{2+} or Ag^{+} (Wen, et al., 2010; He et al., 2010), these biosensors haves some weaknesses. For example, because the fluorescence quenching ability of GO is limited, only low concentrations of DNA probes can be used in GO-based assays for $Hg^{2+}$and Ag^{+}, resulting in narrow linear detection ranges. Despite using low concentrations of DNA probes, these assays suffer from high detection limits. Therefore, much effort is needed to explore new materials for the development of more practical biosensors for Hg^{2+} and Ag^{+} detection.

Herein, a novel dual-color fluorescent biosensing platform based on WS_2 nanosheets was developed for the detection of Hg^{2+} and Ag^{+}. ~~utilizing the excellent fluorescence-quenching capability of WS_2 nanosheet and high specific binding between metal ions and DNA sequences, a simple and effective dual-color fluorescent biosensing platform was developed for homogeneous detection of Hg^{2+} and Ag^{+}.~~ Without added masking agents, the biosensor could achieve simultaneous

detection of Hg^{2+} and Ag^{+} in a high sensitivity and wide linear range. Furthermore, the developed biosensor could simply and conveniently detect Hg^{2+} and Ag^{+} in practical samples. Meanwhile, the possible mechanism of fluorescence quenching by WS_2 nanosheets was carefully studied. This work will contribute to improving capability research of WS_2 nanosheets and extending the application of WS_2 nanosheets to the fields of environmental monitoring and medical diagnosis. ~~The sensitivity and selectivity of the biosensor were evaluated. Simultaneous detection of Hg^{2+} and Ag^{+} coexisting in serum and water samples were also investigated. In addition, the possible mechanism of fluorescence quenching by WS_2 nanosheet was studied. This research extended the application of WS_2 nanosheet in environmental and biological samples monitoring.~~

2. Experimental

2.1. Materials.

Tungsten disulfide (WS_2) nanosheets and graphene oxides were purchased from Nanjing XF Nano Material Tech Co., Ltd. (Nanjing, China). $AgNO_3$, $NaNO_3$, $Hg(NO_3)_2$, $Mg(NO_3)_2$, $Ni(NO_3)_2$, $Co(NO_3)_2$, $Cu(NO_3)_2$, $Mn(NO_3)_2$, $Cd(NO_3)_2$, $Cr(NO_3)_3$, $Pb(NO_3)_2$, $Fe(NO_3)_3$, $Ca(NO_3)_2$, $Zn(NO_3)_2$, $Ba(NO_3)_2$, KNO_3, NaF, $NaClO_4$ and HNO_3(68%) were purchased from Tianjin Guangfu Chemical Reagent Factory

(Tianjin, China). 3-morpholinopropane-sulfonic acid (MOPS) was purchased from Sigma-Aldrich. Hela cells were purchased from the Shanghai Institute of Biochemistry and Cell Biology, Chinese Academy of Sciences. All chemicals and solvents were of analytical grade and were used without further purification. Deionized water was used throughout the experiment. All oligonucleotide sequences were synthesized and purified by Sangon Biotech Co., Ltd. (Shanghai, China).

2.2 Apparatus.

A Hitachi-600 transmission electron microscope (TEM, JEOL, Japan) and field-emission scanning electron microscopy (SEM, Hitachi SU8010, Japan) were used for measuring the morphologies and size of WS_2 nanosheet. Atomic force microscope (AFM, Nanoscope IIIA, USA) were acquired with silicon tips. Fluorescence spectrophotometer (RF-5301PC, Shimadzu, Japan) was used to collect fluorescence spectra. Fluorescence anisotropy and time-resolved fluorescence spectra were conducted on FL920P spectrometer (Edinburgh Instru-ments Ltd, U.K.). The UV-vis absorption was surveyed on a TU-1901 UV-vis spectrophoto-meter (Beijing Purkinje General Instrument Co., Ltd, Beijing, China). Circular dichroism (CD) spectrometer (J-815, Jasco, Japan) was utilized to collect CD spectra.

2.3 Fluorescence assay for detection of Hg^{2+} and Ag^{+}

In the following experiments, all the solutions were prepared in 10

mM MOPS buffer (pH 7.4), which contain~~ing~~ 100 mM $NaNO_3$, 5 mM $Mg(NO_3)_2$). Before detection of $Hg^{2+}$and Ag^{+}, the ~~mixture~~ mixing probe solutions were prepared as follows. FAM-labeled mercury-specific oligonucleotide probes and TAMRA-labeled silver-specific oligonucleotide probes were mixed ~~in a solution and then~~ and incubated for 5 min at 90 °C in order that the secondary structure of the fluorescent probes was completely unwinded (Bian, et al., 2014). Then, the ~~mixture~~ solution was cooled down slowly to the room temperature.

For Hg^{2+} detection, 700 μL above probe solutions ~~first~~ were mixed with 50 μL 0.15 mg/mL WS_2 nanosheets solution at the room temperature for 10 min. Then, different concentrations ~~amounts~~ of target Hg^{2+} solution were added into the reaction mixture to give the final reaction volume of 800 μL. After ~~allowing~~ incubating this mixture ~~to incubate~~ for 20 min at 37 °C, the fluorescence of the mixture was detected. The fluorescence intensity was monitored by exciting the sample at 480 nm and measuring in the range 500-610 nm.

For the Ag^{+} detection, the operation steps were the same with the detection of Hg^{2+}. The fluorescence intensity was monitored by exciting the sample at 530 nm and measuring in the range 560-640 nm.

3. Results and discussion

3.1. Characterization of the WS_2 Nanosheets

~~commercially~~Commercially available ~~bought~~ WS_2 nanosheets were characterized ~~by~~ using TEM, SEM, and AFM. The SEM image revealed that the morphology of WS_2 were two-dimensional thin-layer nanosheets (Fig. ~~S~~1A). Ahigh-resolution TEM image (Fig. ~~S~~1B) and SAED pattern (the insert of Fig. ~~S~~1B) revealed the hexagonal lattice structure with the lattice spacing of 0.27 and 0.16 nm assigned to the (100) and (110) planes (Gutierrez, et al., 2013). WS_2 nanosheets were further confirmed by atomic force microscopy (AFM) images and the height profile (Fig. ~~S~~1C) showed WS_2 nanosheet with about 3.2 nm thickness, suggesting its few-layer structure.

Fig. 1

3.2. Sensing principle

The principle of the sensing platform for the detection of Hg^{2+} and Ag^{+} ~~was displayed~~ is shown in Scheme 1. The ~~mixture~~ mixing probes were used containing ~~composed of~~ mercury-~~ specific DNA probe~~ and silver-specific DNA probes, which were respectively labeled with FAM and TAMRA dyes. These ~~two~~ dye-labeled probes were individually excited at 480 nm and 530 nm to emit green fluorescence and red fluorescence, respectively. In the absence of Hg^{2+} and Ag^{+}, WS_2 nanosheets could easily adsorbed the ~~mixture~~ mixing probe keeping as

free ssDNA via the van der Waals force between nucleobases and the basal plane of WS_2 and then quenched the fluorescence of the two dyes (Xi, et al., 2014; Moses, et al., 2009). So the adsorbed mixed probes exhibited minimal background fluorescence. ~~In contrast~~However, in the presence of Hg^{2+}, the FAM -labeled probe could form mercury- mediated base pairs ("T–Hg^{2+}–T" base pairs), ~~leading to~~ causing form~~ing~~ stable double-stranded DNA (dsDNA) with a hairpin structure (Zhan, et al., 2015; Zhang, et al., 2015). Because the interaction between the formed dsDNA and WS_2 nanosheets became weak, the FAM ~~dye~~-labeled probes whose molecular conformations have been switched would away from the surface of WS_2 nanosheets (Zhu, et al., 2013). As a result, the specific emission of the green color fluorescence (FAM) was recovered while minimal emission of the red color fluorescence (TAMRA) was still maintained. Similarly, when Ag^+ appeared, the TAMRA-labeled probes could also form stable DNA duplexes by C-Ag^+-C base pairs (Bian, et al., 2014). The specific emission of red color fluorescence (TAMRA) was recovered while minimal emission of the green color fluorescence was still maintained. Therefore, by respectively monitoring the fluorescence change of the mixture probes at 525 nm and at 583 nm, the dual-color fluorescent sensing platform based on WS_2 nanosheets provided quantitative readout of the target Hg^{2+} and Ag^+ in the same solution.

Scheme 1

3.3. Feasibility study of the dual-color fluorescent sensing platform

To verify the feasibility of the proposed strategy, several control experiments were performed. Because sulfide can react with Hg^{2+} and Ag^{+} under certain conditions, we first analyzed the changes of the Hg^{2+} and Ag^{+} with ICP-MS when WS_2 nanosheets were added before and after. As shown in table S1 (supporting information), little changes of the Hg^{2+} and Ag^{+} concentrations were observed before and after the addition of WS_2 nanosheets. So Hg^{2+} and Ag^{+} could not react with WS_2 nanosheets in MOPS buffer (pH 7.4). Next, CD measurements were carried out to verify that the designed mixed probe could stably coexist and simultaneously capture Hg^{2+} and Ag^{+} in the same solution, as shown in Fig. ~~1~~2. The original mixed probes containing 1.0 μM FAM-labeled probe and 1.0 μM TAMRA-labeled probe showed strong positive peak at 274 nm, which were the characteristic peaks of ssDNA in accordance with the results of previous studies (Liu, et al., 2009). When 500.0 nM Hg^{2+} was added and incubated with mixed probe, the positive peak at 274 nm obvious decreased in intensity. ~~With the increased concentrations of Hg^{2+} to 1.0 μM~~ When the concentrations of Hg^{2+} were increased to 1.0 μM, the positive peak at 274 nm disappeared and a new negative peak at 277 nm appeared, which indicated forming in a large amount of T-Hg^{2+}-T complexes (Miyake, et al., 2006). Next, when 1.0 μM Ag^{+} was further added and incubated with the mixed probes, the negative peak

continuously increased in intensity and became red-shifted to 279 nm, which indicated the formation of C-Ag^{+}-C complexes (Lin, et al., 2011; Liu, et al., 2009). The above results indicate that the conformation transformation of mixed probes can be induced by Hg^{2+} and Ag^{+} and the designed mixed probes can simultaneously capture Hg^{2+} and Ag^{+} in the same solution. This was crucial for ~~, which is an important basis for~~ establishing dual-color fluorescent sensing platform.

Fig. ~~1~~2

Because fluorescence anisotropy is commonly used to probe weak molecular interactions (He, et al., 2010; Xiao, et al., 2015), to verify WS_2 nanosheets can adsorb the dye-labeled ssDNA mixture and form WS_2 nanosheet complex modified by ssDNA (DNA-WS_2 complexs), the anisotropy measurements were carried out. In the absence of WS_2 nanosheets, the fluorescence anisotropy of free ssDNA mixture was 0.05 (FAM) and 0.13 (TAMRA), respectively. While in the presence of WS_2 nanosheets, the fluorescence anisotropy of ssDNA mixture increased to 0.16 and 0.37, respectively, which indicated ssDNA mixture could be adsorbed onto the surface of WS_2 nanosheets and modified WS_2 nanosheets. After that, the fluorescence quenched assay was carried out to verify WS_2 nanosheet could simultaneously quench the fluorescence of two dyes labeled to mixture probe. As shown in Fig. ~~2~~S1, in the presence of a small amount of WS_2 nanosheets, the fluorescence quenching

efficiency of WS_2 nanosheets to FAM-labeled probe and TAMRA-labeled probe could be achieved to 93.7% and 86.9%, respectively. These results indicate WS_2 nanosheets have ~~strong adsorption ability to ssDNA and~~ high quenching efficiency. Moreover, we have made a comparison of WS_2 nanosheets with grapheme oxide (GO) for fluorescence quenching performance. As shown in Fig. ~~2~~S1, GO (at the same concentration as the WS_2 nanosheets) could not effectively quenched the fluorescence of mixed probes, especially for TAMRA-labeled probes ~~dye~~. To achieve the same quenching degree, ~~the~~ a the 9-fold higher concentration of GO was needed ~~about 9 times concentration~~ than of WS_2 nanosheets. ~~Because of~~ If a very high concentration of quencher is used in the sensing system, the collision efficiency between the fluorescence probes and target ions could be greatly decreased and then the sensitivity of the sensor would reduce. Especially for the quenching-and-recovery-based sensor, this impact was very obvious. Thus, the extraordinarily high quenching efficiency of WS_2 nanosheets is ~~another~~ important ~~basis~~ for establishing the dual-color fluorescent sensing platform.

~~Fig. 2~~

~~Moreover,~~ ~~t~~The possible mechanism of fluorescence quenching by WS_2 nanosheets was further investigated. As shown in Fig. S2A and Fig. S2B, the fluorescence lifetime of these two dyes labeled to mixed probes decreased along with the increase of WS_2 nanosheet amount, which

indicated the occurrence of dynamic quenching. ~~If only the dynamic quenching happened, a~~According to the Stern-Volmer equation, dynamic quenching alone results in a ~~the~~ reduction in fluorescence lifetimes of the two dyes that was equal to decrease ~~the reduction~~ in their fluorescence intensitise (Lakowicz, 2006). However, from the relevant data given in Table ~~S1~~S2 (Supporting Information), it could be found that the fluorescence quenching of these two dyes did not follow ~~properly fit to~~ the Stern-Volmer equation (Fan, et al., 2013). This implied that the fluorescence quenching was not the only mechanism involved. ~~the result of a single mechanism~~. In addition, an obvious red-shift in the emission peak has appeared with adding WS_2 nanosheets (Fig. S3A), ~~which shows~~ indicating that the molecular interactions occurred between WS_2 nanosheets and the two dyes labeled to mixing probes (Fan, et al., 2013; Nagarkar, et al., 2014; Sk, et al., 2014; Ding, et al., 2014). Static quenching might also have occurred ~~exist~~. The Stern–Volmer curves of the quenching system ~~were further studied~~ are shown in ~~(~~Fig. S3B~~)~~. The Stern-Volmer plot exhibited an upward curvature concaving toward the y-axis, which is the characteristic feature of the combination of dynamic and static quenching (Lakowicz, 2006). Thus, the observed quenching effect might be mainly result from the combination of dynamic and static quenching, which is similar to the research conclusion of Liu's group (Yuan, et al., 2014). ~~Therefore, the highly efficient quenching of the dyes~~

~~by WS_2 nanosheet might be caused by the coexistence of both dynamic and static quenching.~~ In addition, because most of 2D nanomaterials, such as graphene oxides and MnO_2 nanosheets could occur energy transfer in interaction with dye-labeled DNA probe (Lu, et al., 2009; Deng et al., 2011), we studied whether there is Förster resonant energy transfer (FRET) in the entire fluorescence suppression process (in supporting information).The results show FRET occur in the fluorescence quenching process of these two dyes by WS_2 nanosheets. Therefore, the possible mechanism of fluorescence quenching by WS_2 nanosheets was related to static quenching, dynamic quenching and FRET coexisting in the entire fluorescence suppression process.

Finally, the proposed strategy was further evidenced by the change of fluorescence spectra under different conditions. As shown in Fig. 3, in the absence of Hg^{2+} and Ag^{+}, the original fluorescence intensities of the mixing probes (curve a_1, curve b_1) was significantly quenched by the WS_2 nanosheets to 6.3% (curve a_{32}) and 13.1% of the original intensity (curve b_{32}) by WS_2 nanosheets, respectively. When 600.0 nM Hg^{2+} was individually added to sensing system, the fluorescence emission intensity of the green color (FAM) was recovered to 51.9% of the original intensity (curve a_{23}), while the red color fluorescence (TAMRA) still kept minimal emission (curve b_4). ~~Meanwhile,~~ Similarly, when 800.0 nM Ag^{+} individually appeared in the sensing system, the fluorescence emission

intensity of the red color (TAMRA) was also recovered to 55.5% of the original intensity (curve b_{23}), while the green color fluorescence (FAM) still kept minimal emission (curve a_4). Furthermore, When 600.0 nM Hg^{2+} and 800.0 nM Ag^{+} were simultaneously added, the fluorescence emission of FAM and TAMRA could still be recovered (curve a_5 and curve b_5). The fluorescence intensity of these two probes were similar to those obtained when Hg^{2+} and Ag^{+} added individually, which indicated Hg^{2+} and Ag^{+} could be detected simultaneously without interfering each other. ~~These~~ Therefore, the fluorescence spectra changes indicate that the proposed sensing platform can be used for ~~individual (or simultaneous)~~ both the individual and simultaneous detection of Hg^{2+} and Ag^{+}.

Fig. 3

3.4. Optimization of assay conditions for detection of Hg^{2+} and Ag^{+}

Before the Hg^{2+} and Ag^{+} detection assay, some important parameters were optimized to obtain the best sensing performance. As the mixing ratio of two fluorescence probes may affect the sensing ability for Hg^{2+} and Ag^{+}, the mixing ratio was optimized. As shown in Fig. S5, the sensing ability was higher for both Hg^{2+} and Ag^{+} when the mixing ratio was 1:1. Thus, the mixing probes including 100 nM FAM-labeled probe and100 nM TAMRA-labeled probe were chosen for further work. ~~The optimization experiments were carried out at a fixed mixture probe concentration of 100 nM in 10 mM MOPS buffer (containing 100 mM~~

~~$NaNO_3$, 5 mM $Mg(NO_3)_2$).~~ Moreover, the concentrations of WS_2 nanosheets used in the assay had a substantial effect on the fluorescence quenching responses. Thus, the concentrations of WS_2 nanosheets were optimized. As shown in Fig. ~~S4~~S6A and Fig. ~~S4~~S6B), the quenching effect was dependent on the concentration of WS_2 nanosheets. ~~In the presence of~~ At a small amount ~~(10 μg/mL)~~ of WS_2 nanosheets (10 μg/mL), the fluorescence of the green color (FAM) was quenched to baseline level, while the fluorescence of the red color (TAMRA) ~~had~~ was not been fully quenched. When the concentration of WS_2 nanosheets was added to15 μg/mL, the fluorescence intensity of the red color (TAMRA) was also quenched to baseline level. Considering Hg^{2+} and Ag^{+} to be detected in same solution, 10 μg/mL was ~~taken~~ used as the optimized concentration for WS_2 nanosheets. The quenching kinetics of the system suggested that the interaction of the dye-labeled ssDNA probe with WS_2 nanosheet was a quite fast process that reached to equilibrium in about 10 min (Fig. ~~S5~~S7). As a result, 10 min was taken as the reaction time for fluorescence quenching of the mixing probe.

The fluorescence response to Hg^{2+} and Ag^{+} was influenced by solution acidity. At a pH below 7.0, protonation of the nitrogen atoms of the thymine base and cytosine base reduces its affinity with Hg^{2+} and Ag^{+} (Wang, et al., 2012), While at relatively higher pH, Hg^{2+} and Ag^{+} may be form complex compounds or precipitates with OH^{-}. Therefore, ~~the effect~~

~~of~~ pH was also optimized. As shown in Fig. ~~S6~~S8, the relative fluorescence change of mixed probe, $(I_F-I_{F0})/I_{F0}$, (where I_{F0} and I_F represent the fluorescence intensity in the absence and presence of Hg^{2+} and Ag^+, respectively.) increased when the pH increased ~~in the range of~~ from 5.0-to7.0. The fluorescence intensity of mixing probes at 525 nm decreased gradually when the pH was higher than 9.0. While the fluorescence intensity of mixing probes at 583 nm gradually decreased when the pH was higher than 7.4. ~~By taking into account~~ In consideration of the performances of the sensing system, ~~pH 7.4 of~~ the 10 mM MOPS buffer solution at pH 7.4 was chosen for further work.

3.5. Performance of the dual-color fluorescent biosensor

The sensitivity of the dual-color fluorescent biosensor for quantitative analysis of Hg^{2+} and Ag^+ was investigated. As shown in Fig. 4A, a dramatic increase in the fluorescence intensity of the green color was observed with the increasing concentration of Hg^{2+} from 6.0 to 650.0 nM. The insert of Fig. 4B shows the relationship between the value of $(I_F-I_{F0})/I_{F0}$ and the Hg^{2+} concentration ~~in the range~~ from 6.0 nM to 450.0 nM (R^2 = 0.996). The limit of detection (LOD) was estimated to be 3.3 nM on the basis of $3\sigma/k$, where σ was the standard deviation for 11 blank samples and k was the slope of calibration line. Fig. 4C shows the fluorescence changes of the red color as increasing the concentration of Ag^+. It could be observed that the value of $(I_F-I_{F0})/I_{F0}$ was dramatically

increased as the Ag^+ concentration increased from 5.0 nM to 1000.0 nM, which showed a good linear relationship in the range of 5 nM to 500.0 nM (R^2 = 0.997) (the insert of Fig.4D) . ~~By~~ Using the same method, the LOD for Ag^+ was estimated to be 1.2 nM. Toxic levels of Hg^{2+} and Ag^+ in drinking water are defined by the United States Environmental Protection Agency (USEPA) to be 72 nM and 460 nM, respectively. In addition, the biological exposure indices (BEIs) for $Hg^{2+}$and Ag^+ defined by American Conference of Governmental Industrial Hygienists (ACGIH) in blood samples are 75 nM and 2 μM, respectively, (Lin, et al., 2011). The LODs for $Hg^{2+}$and Ag^+ in this work are far lower than those set by the organization. Thus, this dual-color fluorescent biosensor is a valuable tool for practical applications.

Fig. 4

To evaluate the specificity of the dual-color fluorescent biosensor, the influence of other environmentally relevant metal ions (including Co^{2+},Cu^{2+}, Cd^{2+}, Pb^{2+}, Mn^{2+}, Ni^{2+}, Cr^{2+}, Fe^{3+}, Ca^{2+}, Zn^{2+}, K^+ , and Ba^{2+}) ~~in the presence of~~ on the sensing system were further investigated. The concentrations of the nonspecific metal ions were 10-fold higher than that of Hg^{2+} and Ag^+. As shown in Fig.5, the ~~higher~~ larger fluorescence enhancement $(I_F-I_{F0})/I_{F0}$ was observed in the presence of Hg^{2+} and Ag^+, while there was very little fluorescence changes in fluorescence caused by ~~the observed in the presence of~~ other metal ions. The selectivity of the

biosensor was also examined with some anions ($\mathbf{NO_3^-}$, $\mathbf{F^-}$, and $\mathbf{ClO_4^-}$), which are often present with free Hg^{2+} and Ag^+ in environment and biological samples. As shown in Figure S9, the fluorescence intensities of anions changed by no more than 8% when anion concentrations were 10-fold and 400-fold higher than that of Hg^{2+} and Ag^+ ions, which further indicated that the developed biosensor is highly selective for Hg^{2+} and Ag^+.

Fig. 5

Compared to ~~with the~~ previously reported work for detection of Hg^{2+} and Ag^+ (Table~~1~~S4), this method ~~exhibited~~ has many advantages. ~~Firstly,~~ This method has a low detection limit for detection of Hg^{2+} and Ag^+. ~~Secondly, c~~ Compared with other methods with similar LODs, ~~the strategy which had a similar detection limit,~~the fluorescent assay has no use of any masking agents for simultaneous detection of Hg^{2+} and Ag^+. ~~It was~~ This method is also very simple. Moreover, the homogeneous assay format makes the assay convenient ~~without~~ because it does not be involve washing or separation steps, ~~and it also~~ which enables this method to be easily automated. The substantial improvement ~~of~~ in the assay's performance were attributed to the following two aspects: (1) The mix-and-detect strategy used ~~independent~~ two independent ~~kinds of~~ specific probes to respectively capture Hg^{2+} and Ag^+, which could avoid the mutual interference for simultaneous detection of Hg^{2+} and Ag^+. (2)

Because WS_2 nanosheets have high quenching efficiency, the interference of background fluorescence in this sensing system could be remarkably reduced. It was beneficial to expanding linearity region of the sensor. At the same time, the sensitivity of the biosensor would be enhanced.

3.6. Detection of Hg^{2+} and Ag^{+} in real samples

In order to further explore the potential applications of the biosensor forreal samples, the standard addition experiment was used to detect Hg^{2+} and Ag^{+} in the tap water， fresh serum，and cell lysate. The results were summarized in Table ~~2~~S5. The recovery of Hg^{2+} and Ag^{+} in the ~~six~~ eight different solutions for each sample was in the range of 90.1−108.3%, and all the relative standard deviations (RSD) were lower than 5.0% (n = 3). These satisfactory results revealed this method could be used to simultaneously (or individually) detect Hg^{2+} and Ag^{+} in water and biological samples.

4. Conclusions

In summary, an effective dual-color fluorescent sensing platform based on WS_2 nanosheet has been developed for homogeneous detection Hg^{2+} and Ag^{+}. The present detection method has several important features. First, ~~taking advantage of~~ it uses the high fluorescence quenching capability of WS_2 nanosheets and excellent specificity of dye-tagged oligonucleotide probes. The sensitively of the present method

was substantially improved with a low detection limit of 3.3 nM and 1.2 nM for Hg^{2+} and Ag^{+}, respectively, which were lower than most reported assays. Second, the homogeneous assay format made the assay convenient without requiring washing or separation steps, and it also enabled this method to be easily automated. ~~Third~~Finally, compared to the previous reported assays for simultaneous detection of Hg^{2+} and Ag^{+}, this method was no use of any masking agents and relatively simple. These merits greatly endowed this method held a promise ~~in~~ for monitoring heavy metal ions in environmental and biological samples.

Acknowledgment

The authors are grateful for financial support from the National Natural Science Foundation of China (No. 21375053, 21405066) and the Specialized Research Fund for the Doctorial Program of Higher Education (No. 20130211110039).

References:

Aragay, G., Pons, J., Merkoci, A. 2011.Chem. Rev. 111, 3433−3458.

Bian, L., Xu, J., Hu,W., 2014. J. Agric. Food Chem. 62, 4870-4877.

Chhowalla, M., Shin, H. S., Eda, G., Li, L. J., Loh, K. P., Zhang, H., 2013. Nat. Chem. 5, 263-275.

Chou, S. S., De, M., Kim, J., Byun, S., Dykstra, C., Yu, J., Huang, J.,

504 Dravid, V. P., 2013. J. Am. Chem. Soc. 135, 4584-4587.
505 Chu, K. W., Chow, K. L. Aquat., 2002.Toxicol. 61, 53-64.
506 Cizdziel, J. V., Gerstenberger, S., 2004.Talanta 64, 918-921.
507 Coleman, J. N., Lotya, M., O'Neill, A., Bergin, S. D., King, P. J., Khan,
508 U., Young, K., Gaucher, A., De, S., Smith, R. J., Shvets, I. V., Arora,
509 S. K., Stanton, G., Kim, H.-Y., Lee, K., Kim, G. T., Duesberg, G. S.,
510 Hallam, T., Boland, J. J., Wang, J. J., Donegan, J. F., Grunlan, J. C.,
511 Moriarty, G., Shmeliov, A., Nicholls, R. J., Perkins, J. M., Grieveson,
512 E. M., Theuwissen, K., McComb, D. W., Nellist, P. D. Nicolosi, V.,
513 2011. Science 331,568-571
514 Deng, R., Xie, X., Vendrell, M., Chang, Y. T., Liu, X., 2011. J. Am. Chem.
515 Soc. 133, 20168−20171.
516 Ding, A., Yang, L., Zhang, Y., Zhang, G., Kong, L., Zhang, X., Tian, Y.,
517 Tao, X., Yang, J., 2014. Chem.Eur. J. 20, 12215−12222.
518 Fan, K., Guo, Z., Geng, Z., Ge, J., Jiang, S., Hua, J., Zhang, Q., 2013.
519 Chinese Physical Society 26, 252-258.
520 Gutierrez, H. R., Perea-Lopez, N., Elias, A. L., Berkdemir, A., Wang, B.,
521 Lv, R., Lopez-Urias, F., Crespi, V. H., Terrones, H., Terrones, M.,
522 2013. Nano Lett. 13, 3447-3454.
523 He, S., Song B., Li D., Zhu, C., Qi, W., Wen, Y., Wang, L., Song, S., Fang,
524 H., Fan, C., 2010. Adv. Funct. Mater. 20, 453–459.
525 Lu, C-H., Yang, H-H., Zhu, C-L., Chen, X., Chen, G-N., 2009. Angew.

526 Chem. 121, 4879 –4881.

527 Huang, K.-J., Liu, Y.-J.,Wang, H.-B.,Gan, T., Liu, Y.-M.,Wang, L.-L,

528 2014. Sens. Actuators, B: Chem. 191, 828-836.

529 Jitaru, P., Tirez, K., De Brucker, N., 2003. At. Spectrosc. 24, 1-10.

530 Li, H., Zhai, J., Tian, J., Luo, Y., Sun, X., 2011. Biosens. Bioelectron.

531 26, 4656-4660.

532 Lin, Z., Li, X., Kraatz, H.-B., Anal. Chem. 2011, 83, 6896-6901.

533 Lin, C.-Y., Yu, C.-J., Lin, Y.-H., Tseng, W.-L., 2010. Anal. Chem. 82,

534 6830-6837.

535 Lin, T., Zhong, L., Song, Z., Guo, L., Wu, H., Guo, Q., Chen, Y., Fu, F. F.,

536 Chen, G., 2014. Biosens. Bioelectron. 62, 302-307.

537 Liu, C., Huang, C., Chang, H., 2009. Anal. Chem. 81, 2383-2387.

538 Liu, H., Wang, Y., Shen, A., Zhou, X., Hu, J., 2012.Talanta 93, 330-335.

539 Lakowicz, J., 2006. Principles of Fluorescence Spectroscopy, in:

540 Lakowicz, J. (Eds.), Quenching of Fluorescence, Springer, New York,

541 pp. 278-283.

542 Miyake, Y., Togashi, H., Tashiro, M., Yamaguchi, H., Oda, S., Kudo, M.,

543 Tanaka, Y., Kondo, Y., Sawa, R., Fujimoto, T., Machinami, T., Ono,

544 A., 2006. J. AM. CHEM. SOC. 128, 2172-2173.

545 Moses, P. G., Mortensen, J. J., Lundqvist, B. I., Nørskov, J. K., 2009. J.

546 Chem. Phys. 130, 104709 (6 pages).

547 Nagarkar, S. S., Desai, A. V., Ghosh, S. K., 2014. Chem. Commun.

548 50, 8915-8918.
549 Ono, A., Cao, S., Togashi, H., Tashiro, M., Fujimoto, T., Machinami, T.,
550 Oda, S., Miyake, Y., Okamoto, I., Tanaka, Y., 2008. Chem. Commun.
551 44, 4825-4827.
552 Pu, Q. S., Sun, Q. Y., Hu, Z. D., Su, Z. X., 1998. Analyst 123, 239-243.
553 Qin, Y., Ma, Y., Jin, X., Zhang, L., Ye, G., Zhao, S., 2015. Anal. Chim.
554 Acta. 866, 84-89.
555 Ratte, H. T. Environ. 1999. Toxicol. Chem. 18, 89-108.
556 Shi,W., Sun, S., Li, X., Ma, H., 2010. Inorg. Chem. 49, 1206-1210.
557 Sk, M. P., Chattopadhyay, A., 2014. RSC Adv. 4, 31994-31999.
558 Tan, S. S., Teo, Y. N., Kool, E. T., 2010. Org. Lett. 12, 4820-4823.
559 Wang, H., Kim, Y., Liu, H., Zhu, Z., Bamrungsap, S., Tan, W., 2009.
560 J. Am. Chem. Soc. 131, 8221-8226.
561 Wang, S., Si, S., 2013. Anal. Methods 5, 2947-2953.
562 Wang, Y., Zheng, Y., Yang, F. and Yang, X., 2012. Chem Commun
563 (Camb), 48, 2873-2875.
564 Wang, Z.-X., Ding, S.-N., 2014. Anal. Chem. 86, 7436-7445.
565 Wen, Y., Xing, F., He, S., Song, S., Wang, L., Long, Y., Li, D., Fan, C.,
566 2010. Chem. Commun. 46, 2596-2598.
567 Wu, L.-L., Wang, Z., Zhao, S., Meng, X. Song, X.-Z., Feng, J. Song,
568 S.-Y., Zhang, H.-J., Chem. Eur. J. 2016, 22, 477-480.
569 Xi, Q., Zhou, D.-M., Kan, Y.-Y., Ge, J., Wu, Z.-K., Yu, R.-Q., Jiang, J.-H.,

570 2014. Anal. Chem. 86, 1361-1365.

571 Xia, J., Lin, M., Zuo, X., Su, S., Wang, L., Huang, W., Fan, C., Huang, Q.,

572 Anal. Chem. 2014, 86, 7084-7087.

573 Xiao, X., Li, Y. F., Huang , C.Z., Zhen, S. J., 2015. Chem. Commun. 51,

574 16080-16083.

575 Yuan, Y., Li, R., Liu, Z., 2014. Anal. Chem. 86, 3610-3615

576 Zeng, Z., Yin, Z., Huang, X., Li, H., He, Q., Lu, G., Boey, F., Zhang H.,

577 Angew. Chem. Int. Ed. 2011, 50, 11093-11097.

578 Zhan, S., Xu, H., Zhang, D., Xia, B., Zhan, X., Wang, L., Lv, J., Zhou, P.,

579 2015. Biosens. Bioelectron. 72, 95-99.

580 Zhang, J. R., Huang, W. T., Zeng, A. L. , Luo, H. Q., Li, N. B., 2015.

581 Biosens. Bioelectron. 64, 597-604.

582 Zhang, X., Li, Y., Su, H., Zhang, S. 2010. Biosens. Bioelectron. 25,

583 1338-1343.

584 Zhang, Y., Jiang, H., Wang, X., 2015. Anal. Chim. Acta 870, 1-7.

585 Zhao, J., Ma, Y., Kong, R., Zhang, L., Yang, W., Zhao, S., 2015. Anal.

586 Chim. Acta 887, 216-223.

587 Zhu, C., Zeng, Z., Li, H., Li, F., Fan, C., Zhang, H., 2013. J. Am. Chem.

588 Soc. 135, 5998-6001.

589 Zhu, G., Lia, Y., Zhang, C.-y., 2014. Chem. Commun. 50, 572-574.

590 Zhu, G. C., Zhang, C. Y., 2014. Analyst, 139, 6326-6342.

591

Figure

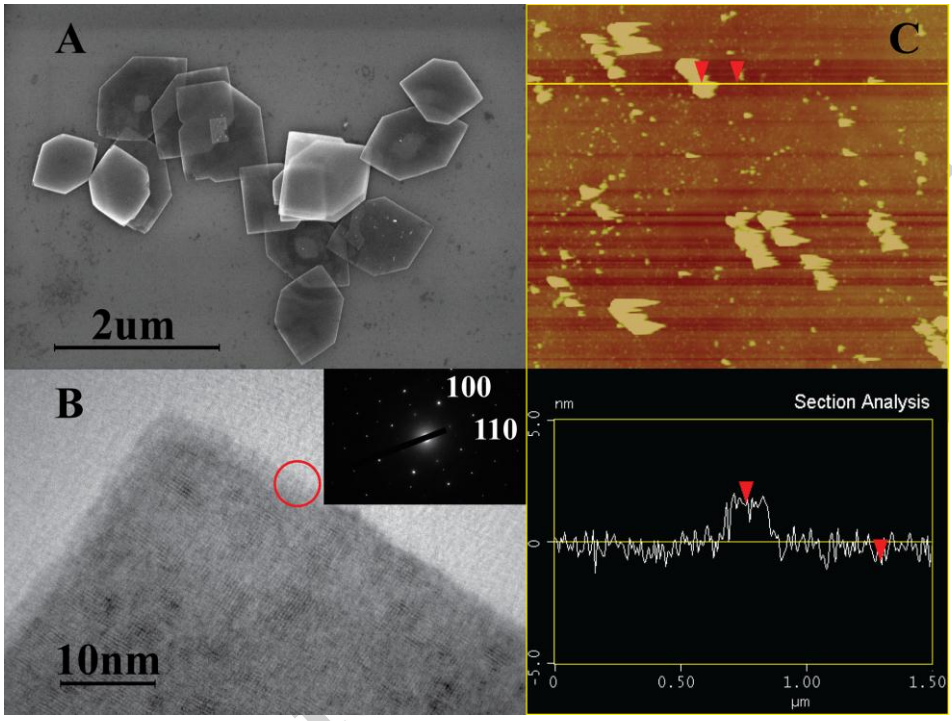

Fig. 1 (A) SEM image of WS_2 nanosheets, (B) HRTEM image of WS_2 nanosheets, Inset: EDS spectrum of WS_2 nanosheets, (C) AFM image and height profile of WS_2 nanosheets.

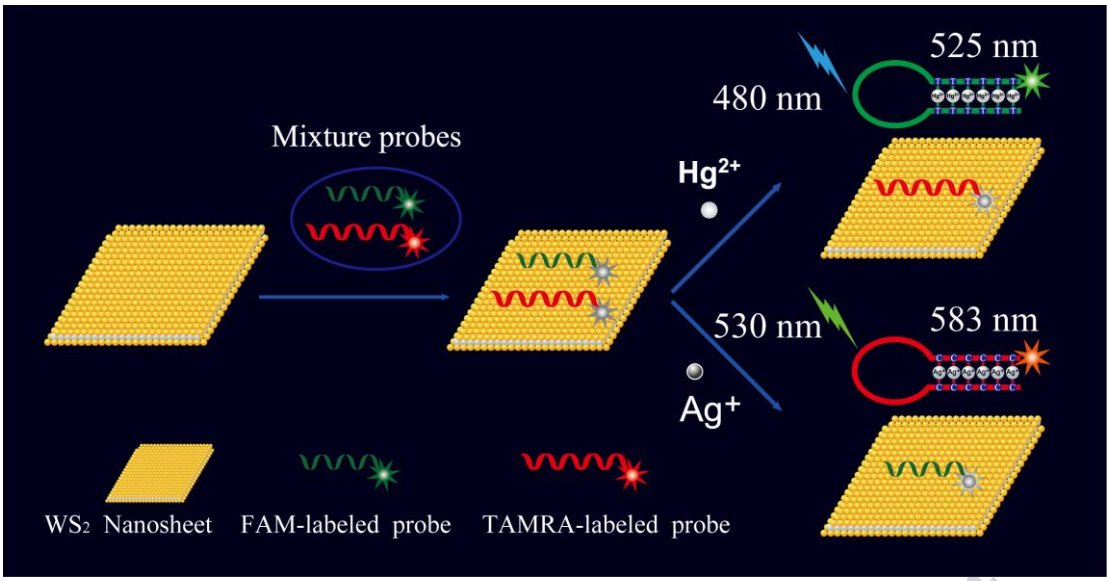

Scheme 1. Schematic illustration of WS_2 nanosheet-based sensing platform for dual-color fluorescent analysis of Hg^{2+} and Ag^{+}. Fluorescence spectra of mixing probe in the presence of different targets Hg^{2+} (green) and Ag^{+} (red) with the excitation wavelengths of 480 and 530 nm, respectively.

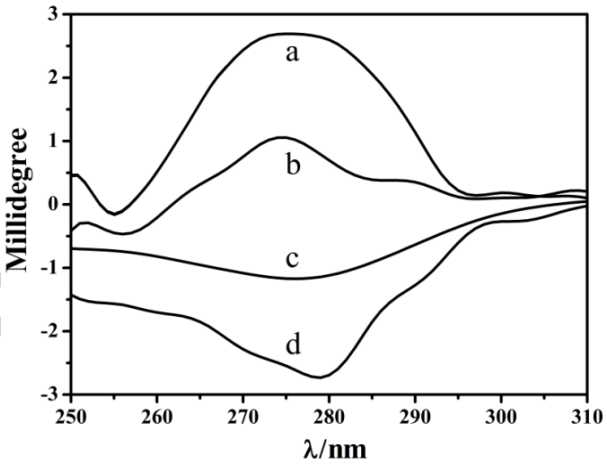

Fig. ~~1~~2 CD spectral change of ~~mixture~~ mixing probe containing 1.0 μM FAM dye-labeled probe and 1.0 μM TAMRA dye-labeled probe in the presence of increasing Hg^{2+} and Ag^{+} concentrations. (a) mixing probes , (b) mixing probes + 500.0 nM Hg^{2+}, (c) mixing probes + 1.0 μM Hg^{2+} , (d) mixing probes +1.0 μM Hg^{2+}+1.0 μM Ag^{+}.

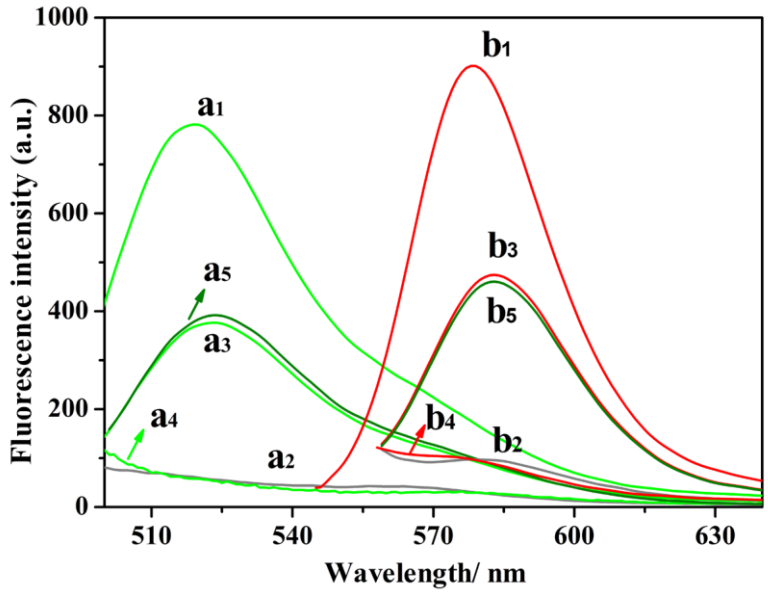

Fig. 3 Fluorescence spectra for dual-color detection of Hg^{2+} and Ag^{+}.（A）Fluorescence spectra of the green color (FAM) at different conditions: (a_1) ~~mixture probe~~ mixing probes, (a_2) mixing probes+WS_2, (a_3) mixing probes +WS_2+Hg^{2+}(600.0 nM), (a_4) mixing probes +WS_2+Ag^{+}(800.0nM), (a_5) mixing probes +WS_2+Hg^{2+}(600.0nM)+Ag^{+} (800.0 nM); (B) Fluorescence spectra of the red color (TAMRA) at different conditions: (b_1) mixing probes, (b_2) mixing probes +WS_2, (b_3) mixing probes +WS_2 + Ag^{+}(800.0 nM), (b_4) mixing probes +WS_2+Hg^{2+}(600.0 nM), (b_5) mixing probes +WS_2+ Hg^{2+}(600.0 nM)+Ag^{+}(800.0 nM). Mixing probes: 100 nM FAM-labeled probe and 100 nM TAMRA dye-labeled probe, WS_2 nanosheets: 10μg·mL^{-1}.

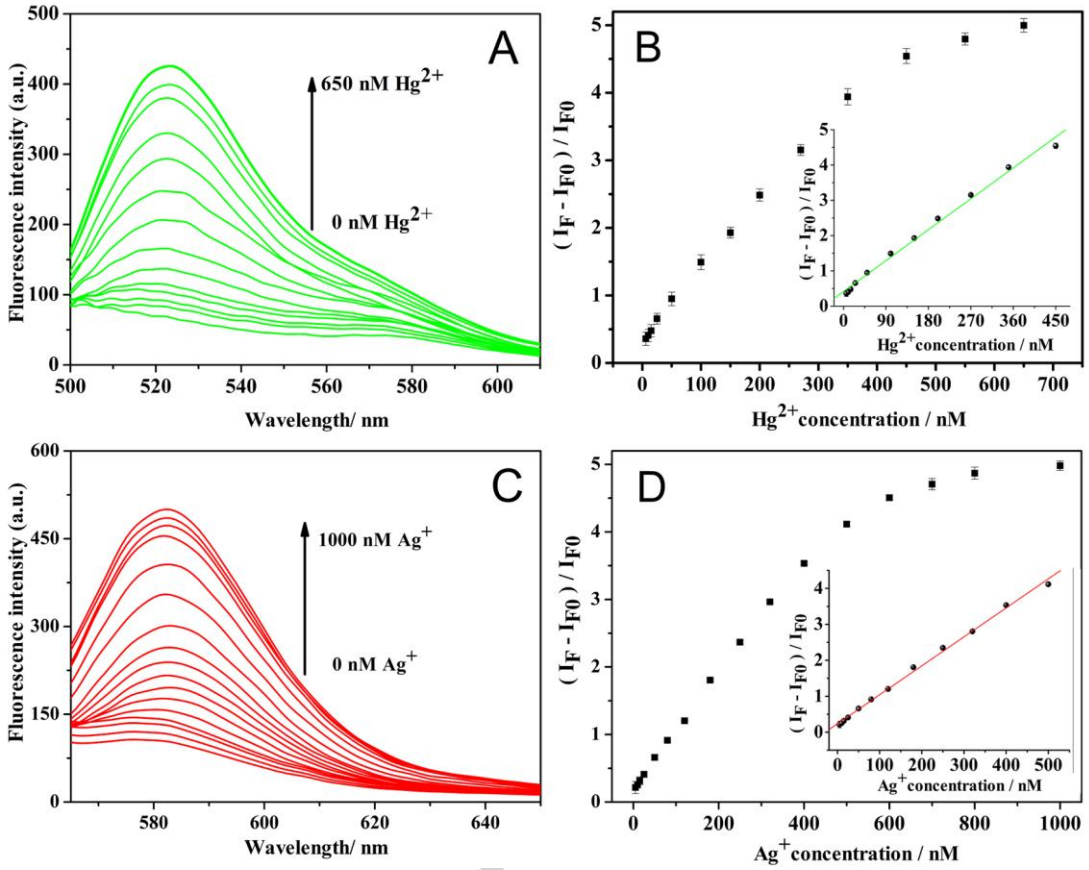

Fig. 4 (A) Fluorescence emission spectra of FAM ~~the green color~~ in the presence of different concentrations of Hg^{2+} (0, 6.0, 10.0, 15.0, 25.0, 50.0, 100.0, 150.0, 250.0, 270.0, 350.0, 450.0, 550.0 and 650.0 nM). (B) Calibration curve for Hg^{2+} detection. (C) Fluorescence emission spectra of TAMRA ~~the red color~~ in the presence of different concentrations of Ag^{+} (0, 5.0, 10.0, 15.0, 25.0, 50.0, 80.0, 120.0, 180.0, 250.0, 320.0, 400.0, 500.0, 600.0, 700.0, 800.0, and 1000.0 nM). (D) Calibration curve of Ag^{+} detection.

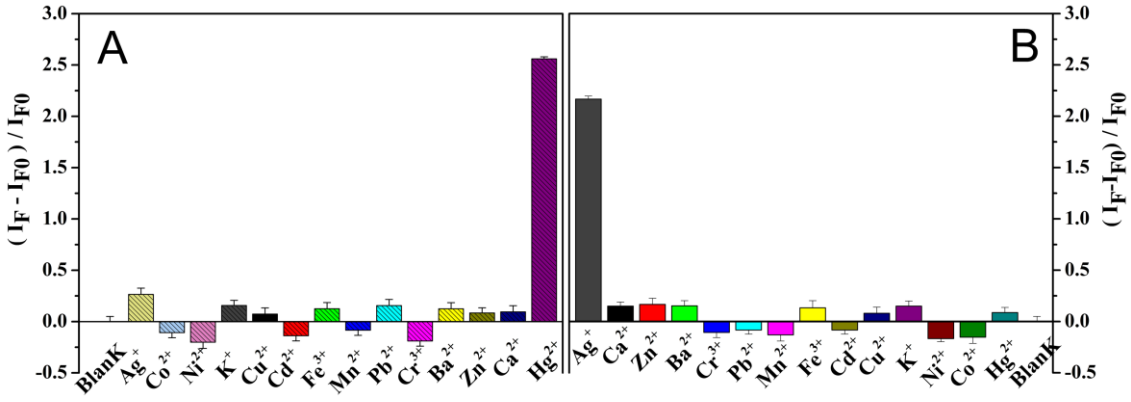

Fig. 5 Selectivity of the sensing system for detection of Hg^{2+} and Ag^{+} in the presence of the other metal ions. (A) ~~The s~~Specificity ~~for~~ of Hg^{2+} detection. (B) ~~The s~~Specificity ~~for~~ of Ag^{+} detection. The concentrations of both Hg^{2+} and Ag^{+} were 250.0 nM, and those of the other metal ions were 2.5 μM.

Highlights

- WS_2 nanosheet was demonstrated to develop a dual-color fluorescent biosensing platform for detection of Hg^{2+} and Ag^{+}.
- Without ~~adding~~ using any masking agents, the biosensor could achieve simultaneous detection of Hg^{2+} and Ag^{+} with a low detection limit.
- The homogeneous assay format made this method simple and convenient.
- ~~The coexistence of both dynamic and static quenching caused the highly efficient quenching of the dyes labeled to DNA probe.~~